Published in final edited form as:
Free Radic Biol Med. 2009 October 1; 47(7): 992–1004. doi:10.1016/j.freeradbiomed.2009.07.001.

Anti-angiogenic action of redox modulating Mn(III) *ortho* tetrakis *N*-ethylpyridylporphyrin, MnTE-2-PyP^{5+}*via* suppression of oxidative stress in a mouse model of breast tumor

Zahid N. Rabbani[1], **Ivan Spasojevic**[3], **XiuWu Zhang**[1], **Benjamin J. Moeller**[1,a], **Sinisa Haberle**[3], **Jeannette Vasquez-Vivar**[2], **Mark W. Dewhirst**[1], **Zeljko Vujaskovic**[1,*], and **Ines Batinic-Haberle**[1,*]

[1] Department of Radiation Oncology, Duke University School of Medicine, Durham, NC 27710

[2] Department of Biophysics, Medical College of Wisconsin Milwaukee, WI 53226-0509

[3] Department of Medicine, Duke University School of Medicine, Durham, NC 27710

Abstract

MnTE-2-PyP^{5+} is a potent catalytic scavenger of reactive oxygen and nitrogen species, primarily superoxide and peroxynitrite. It therefore not only attenuates primary oxidative damage, but was found to modulate redox-based signaling pathways (HIF-1α, NF-κB, SP-1 and AP-1), and thus in turn secondary oxidative injury also. Cancer has been widely considered as an oxidative stress condition. The goal of the present study was to prove if and why a catalytic SOD mimic/peroxynitrite scavenger would exert anti-cancer effects; i.e. to evaluate whether the attenuation of the oxidative stress by MnTE-2-PyP^{5+} could suppress tumor growth in a 4T1 mouse breast tumor model. Tumor cells were implanted into Balb/C mouse flanks. Three groups of mice (n=25) were studied: control (PBS), 2 mg/kg/day and 15 mg/kg/day of MnTE-2-PyP^{5+} given subcutaneously twice daily starting when the tumors averaged 200 mm^3 (until they reached ~5-fold of initial volum). Intratumoral hypoxia (pimonidazole, carbonic anhydrase, CAIX), HIF-1α, VEGF, proliferating capillary index (CD105), microvessel density (CD31), protein nitration, DNA oxidation (8-OHdG) NADPH oxidase (Nox-4), apoptosis (CD31), macrophage infiltration (CD68) and tumor drug levels were assessed. With 2 mg/kg/day a trend toward tumor growth delay was observed and was significant with 15 mg/kg/day. The 7.5-fold increase in drug dose was accompanied by similar (6-fold) increase in drug tumor levels. Oxidative stress was largely attenuated as was observed through the decreased levels of DNA damage, protein 3-nitrotyrosine, macrophage infiltration and NADPH oxidase. Further, hypoxia was significantly decreased as were the levels of HIF-1α and VEGF. Consequently, suppression of angiogenesis was observed; both the microvessel density and the endothelial cell proliferation were markedly decreased. Our study indicates for the first time that MnTE-2-PyP^{5+} has anti-cancer activity in its own right. The anti-cancer activity *via* HIF/VEGF pathways probably arises from the impact of the drug on the oxidative stress. Therefore, the catalytic scavenging of ROS/RNS by antioxidants, which in turn suppresses cellular transcriptional activity, could be an appropriate strategy for anti-cancer therapy. Enhancement of the anti-cancer effects may be achieved by

*Corresponding authors: Ines Batinic-Haberle, Ph. D., Department of Radiation Oncology-Cancer Biology, Duke University Medical Center, Research Drive, 281b/285 MSRB I, Box 3455, Durham, NC 27710, Tel: 919-684-2101, Fax: 919-684-8718, ibatinic@duke.edu, Zeljko Vujaskovic, MD, PhD, Duke University Medical Center, 201 MSRB, Box 3455, Durham, NC 27710, Tel: 919-681-1675, Fax: 919-684-8718, vujas@radonc.duke.edu.
[a]Present address: MD Anderson, 4749 Kingfisher Drive, Houston, TX 77035

optimizing the dosing regime, utilizing more bioavailable Mn porphyrins (MnP), and combining MnP treatment with irradiation, hyperthermia and chemotherapy. Mn porphyrins may be advantageous compared to other anti-cancer drugs, due to their radioprotection of normal tissue and the ability to afford pain management *via* prevention of chronic morphine tolerance.

Keywords

anti-cancer (anti-tumor) therapy; SOD mimic; peroxynitrite scavenger; Mn porphyrin; MnTE-2-PyP^{5+} (AEOL10113); HIF1-α; VEGF; cancer biology; oxidative stress; angiogenesis; inflammation

Introduction

Cationic Mn porphyrins (MnP) bearing electron-withdrawing positively charged groups close to the metal center exert both thermodynamic and electrostatic facilitation of the reaction with anionic superoxide and peroxynitrite and are thus among the most potent scavengers of those species [1–8]. They have been originally developed based on structure-activity relationships between the catalytic rate constant for $O_2^{\cdot -}$ dismutation and the metal-centered redox potential [2,6,8]. It has been later shown that their ability to scavenge $O_2^{\cdot -}$ parallels their efficacy in reducing $ONOO^-$, both being catalytic in nature [9,10]. The most potent cationic *beta* and *meso* substituted quaternized Mn(III) *N*-pyridylporphyrins have metal-centered reduction potential around the midway potential for the $O_2^{\cdot -}$ reduction and oxidation similar to SOD enzymes ($E_{1/2}$ = ~ + 300 mV *vs.* NHE). In addition, those Mn porphyrins afford electrostatic facilitation for the reaction with $O_2^{\cdot -}$ which results in k_{cat} that approaches or equals the k_{cat} of the SOD enzymes themselves [6,8,11]. Such positive potentials make $Mn^{III}P$ readily reducible with cellular reductants such as ascorbate and tetrahydrobiopterin [9,10,12]. *Via* one- or two-electron oxidation with O_2^- or $ONOO^-$, respectively, Mn porphyrin in its reduced state ($Mn^{II}P$) would *in vivo* behave as a superoxide [12], or peroxynitrite reductase, rather than as an SOD mimic.

The most potent among Mn porphyrins, MnTE-2-PyP^{5+} (Figure 1), MnTnHex-2-PyP^{5+}, and MnTDE-2-ImP^{5+} [2,4,5] proved effective in different animal models of oxidative stress [13–25]. As our insight into the efficacy of these compounds and their mechanism of action *in vivo* increases along with our understanding that oxidative stress is a factor in cancer, aging, central nervous system disorders and other diseases, it became obvious that Mn porphyrins *(a)* decrease the primary oxidative damage to biological targets and *(b)* suppress the redox-based cellular transcriptional activity which would otherwise result in activation of inflammatory and immune responses that would amplify the primary oxidative event. Both actions likely stem from the elimination of the signaling ROS/RNS and are based on favorable redox properties of Mn porphyrins. We have shown significant to full (brought to control levels) suppression of the major transcription factors AP-1 [22], SP-1 [21], NF-κB [14,21] and HIF-1α [18] by MnTE-2-PyP^{5+} (Figure 1), which was accompanied with decreased levels of related inflammatory cytokines. Suppression of all four pathways is relevant in tumor growth as we have already shown with skin cancerogenesis (AP-1) and tumor radiosensitization studies (HIF-1α). Activation of HIF-1α by reactive species H_2O_2, .NO and/or $ONOO^-$ is fully prevented by MnTE-2-PyP^{5+}, which in turn results in suppression of VEGF and bFGF [18]. Suppression of HIF-1α stabilization by .NO [26] may also play a role. In a 4T1 breast tumor mouse model, MnTE-2-PyP^{5+} was further reported to be an effective tumor radiosensitizer, augmenting the radiation-induced damage to the tumor vasculature [17,27]. When irradiated, due to enhanced production of reactive species, tumors “in their efforts to survive”, upregulate HIF-1α and VEGF to support new vasculature and thus tumor growth [17,27]. Again, by removing reactive species, MnTE-2-PyP^{5+} inhibits HIF-1α activation and VEGF expression, consequently causing a significant suppression of tumor angiogenesis/growth [17,18].

It is well-documented that tumors are under oxidative stress which is a driving force that promotes tumor growth [28]. The major cellular antioxidant defense, mitochondrial MnSOD, was shown to modulate tumor growth [29–32]. The mechanistic explanations of such effects that have been offered, including those by the Oberly and Melendez groups are complex [33–40]. When tumor is irradiated, one would expect that Mn porphyrin, if any, would protect it *via* its basic antioxidant function whereby decreasing levels of ROS/RNS, suppressing tumor oxidative stress and in turn preventing tumor growth. While this likely occurs to some degree, the other, anti-angiogenic action of MnP *via* suppression of transcriptional activity *i.e.* suppression of vasculature growth prevails. Consequently MnTE-2-PyP^{5+} is not tumor-protective [17,27].

The radioprotection of normal tissue by Mn porphyrins [17,18,26,29], along with anti-cancer effects observed in this study, would allow these drugs to exert dual actions in tumor therapy. The efficacy in preventing chronic morphine tolerance was recently reported [25]. It would add another dimension to the use of Mn porphyrins in tumor therapy – pain management, which along with radioprotectiveness would make these drugs advantageous over other anti-cancer agents.

Our goal herein was to further our understanding of the impact of MnTE-2-PyP^{5+}, in its own right, on tumor growth suppression through modulation of induction of HIF-1α/VEGF pathways on murine breast tumor.

Materials and Methods

Mouse tumor model and treatment

Balb/C mice (Charles River Laboratories, Wilmington, MA) were housed and treated in accordance with approved guidelines from the Duke University Institutional Animal Care and Use Committee. The animals were allowed to adapt to the laboratory environment for 7 days before experiments.

4T1 cells were routinely cultured in Dulbecco's Modified Eagle's medium (DMEM) containing 10% fetal bovine serum (FBS). 4T1 tumors were grown in the flank of mice by injecting a suspension of 10^6 tumor cells/mouse. Tumor volumes were measured with calipers and calculated according to two diameters with the formula: $V = (a^2 \times b)/2$, where V is the volume, a is the short diameter, and b is the long diameter.

MnTE-2-PyP^{5+} was synthesized as previously described [2]. The compound was prepared in a sterile phosphate-buffered saline (PBS) and administered twice daily by subcutaneous (s.c.) injections (low dose, 2 mg/kg/day and high dose, 15 mg/kg/day). Animals were randomly assigned to three treatment groups with 25 mice per group: control (PBS), low dose and high dose of MnTE-2-PyP^{5+}. Treatment started when tumors size averaged 200 mm^3 (day 0). Mice received on average 80 μL of the solution, the volume adjusted to the increasing weight of the animal. No sign of toxicity was observed with either dose. The tumor growth and animal weight were followed on alternate days. When the tumor volume reached 5 fold of initial volume, the animals were injected with pimonidazole and sacrificed three hours later. The tumors were harvested (snap frozen) and stored at −80 °C for further processing.

Immunohistochemistry

Using a LEICA CM 1850 cryotome (Meyer Instruments Inc., Houston, TX), tumors were cut into 10–12 μm frozen sections, and adhered to Poly-L-Lysine coated slides. The sections were fixed in 4% paraformaldehyde in PBS (pH 7.2) for 45 minutes, then blocked with 10 % normal serum. The following primary antibodies were applied: rabbit polyclonal anti-VEGF (Santa Cruz Biotechnology, Santa Cruz, CA), mouse monoclonal anti-carbonic anhydrase IX (CAIX;

gift from Dr. Oosterwijk), mouse monoclonal anti-HIF-1α (Novus Biological, Littleton, CO, USA) rabbit polyclonal pimonidazole (gift from Dr. James Raleigh), rat monoclonal anti-CD31, CD105 and CD68 (BD Pharmingen, San Jose, CA, USA), goat polyclonal against homologue of $gp91^{phox}$ catalytic subunit of phagocyte NAD(P)H oxidase (Nox-4), mouse monoclonal anti 8-OHdG (1:2000, JaICA, Shizuoka, Japan), mouse monoclonal anti 3-nitrotyrosine (Santa Cruz Biotechnology, Santa Cruz, CA), rabbit monoclonal anti-caspase 3 (Cell Signaling Technology Inc., Danvers, MA, USA) and rabbit polyclonal Ki-67 (Vector Laboratories, Burlingame, CA, USA). Omission of the primary antibody served as negative control. Biotinylated donkey anti-rabbit, goat or anti-mouse secondary antibodies were used where relevant. The ABC kit and Nova-Red solution (Vector Laboratories, Burlingame, CA, USA) were used according to manufacturer's recommendations. Slides were counterstained with Harris hematoxylin and mounted with coverslips.

The relative expressions of VEGF, CAIX, pimonidazole, Nox-4, and nitrotyrosine, in treated versus control tumors were calculated from the quantification of digitized images [positively-stained area (brown staining) and total area per low power field (Adobe Photoshop)]. Microvessel density (MVD) and proliferating capillary index (PCI) was calculated at lower magnification and CD31/105-positive vessels were counted in each tumor xenograft from 4–5 random fields. Vascular hot spots were also identified, and individual microvessel counts were made on a 100X field. Any highlighted endothelial cell or cell group occurring closely together and distinctly apart from microvessels, tumor cells, or other near-lying connective tissue morphology, was defined as a singular microvessel count. Results were expressed as the highest number of microvessels in any single 100X field. Tumor cells with intranuclear staining were considered positive for HIF-1α. After the slides were scanned at low magnification (40X), positive cells were counted in 4–5 random fields at a magnification of 400X (NIH Image J). The total number of cells in the respective fields was also determined to derive labeling index for HIF-1α.

Double immunofluorescent immunohistochemistry

The slides were incubated sequentially with the following primary antibodies: CD31 (1:200, rat anti mouse, BD Pharmingen), CD68 (1:200, rat anti mouse, BD Pharmingen), nitrotyrosine and Nox-4 (1:250 and 1:200, Santa Cruz biotechnology). FITC and TRITC labeled secondary antibodies (Jackson Immuno-research) were applied respectively. The tumor sections were digitized with a computerized digital image analysis system. A high resolution, intensified solid state camera on a fluorescence microscope (Axioskop, Zeiss) was used. Each tumor field was sequentially scanned two times at 100 magnification, using two different filters for the FITC (green), and Texas red (red) signals to identify double staining. Then respective stains were overlayed by using Metamorph software (Universal Imaging Corporation).

Protein Extraction and Western Blot

The snap frozen tumor tissues were homogenized in 500 μl ice-cold buffer containing 1% sodium dodecylsulfate, 5 mM Tris-HCl (pH 7.4), 2 mM EDTA, 10μg/ml aprotinin, and 0.5 mM phenylmethylsulfonyl fluoride. Samples were sonicated on ice for 15 sec and centrifuged at 12,000 × g for 5 min at 4°C to remove large tissue debris. Protein concentrations were determined by the Bradford assay [41]. In preparation for Western blotting, the lysate was diluted 6-fold with sample buffer [480 ml/L glycerol, 60g/L SDS, 17.28 mM β-mercaptoethanol, 12 mM EDTA, 300 mmol/L Tris-HCl (pH 6.8), 0.1g/L bromophenol blue], and boiled for 5 min. After running, PAGE gels were incubated with anti-HIF-1α antibody (1:500 dilution; Novus Biological, Littleton, CO) for 3 hrs, and blots were washed, and then incubated with peroxidase-labeled anti-mouse antibody (1:5,000; y) for 2 hrs. The blots were developed with Chemiluminescent substrate (Pierce Chemical Company, Rockford, IL, USA).

To control for loading efficiency, blots were re-probed for α-tubulin. Western blot data were quantified as described [42].

Determination of MnTE-2-PyP^{5+} levels in tumor

MnTE-2-PyP^{5+} was determined as previously described for the analysis of its mitochondrial levels and pharmacokinetic study [43,44]. After tumors were homogenized with 1 + 2 volumes of water, and proteins removed, MnTE-2-PyP^{5+} was reduced to MnTE-2-PyP^{4+} by ascorbate. The exchange of Mn site by Zn was followed by HPLC/fluorescence analysis of ZnTE-2-PyP^{5+}. Three tumors from low-dose and high-dose groups were analyzed.

Statistics

Results are expressed as means ± SEM Student's t test. $P<0.05$ was considered statistically significant.

Results

MnTE-2-PyP^{5+} has anti-tumor effects

There was a trend towards tumor growth delay by this compound with low dose (p=0.06), but was significant with high dose (p=0.002) (Figure 2). The suppression of tumor growth became obvious at later time points when tumor vasculature starts growing to support exponential tumor growth. At a high dose tumor growth ceased at 14 days. No differences in weight gain among groups were observed (data not shown).

Levels of MnTE-2-PyP^{5+} in tumors

Tumor accumulation of MnTE-2-PyP $^{5+}$ occurred in a dose dependent manner (Table 1). The 7.5-fold increase in drug dose was paralleled by 6-fold increase in drug tumor levels.

MnTE-2-PyP^{5+} decreases tumor oxidative stress and inflammatory response

NADPH oxidase (Nox-4) was significantly reduced in low-and high dose-groups (p=0.01 and p=0.003) (Figure 3). In comparison, PBS-treated tumors displayed strong immunoreactivity. DNA oxidation assessed by 8-OHdG immunohistochemistry, revealed strong staining in control tumors (Figure 3). A significant reduction in DNA oxidation was seen in low and high dose groups (p=0.01and p=0.009) (Figure 3). Tumor sections from PBS-treated mice displayed strong immunoreactivity for the presence of protein 3-nitrotyrosine. Thus, diffusely positive cytoplasmic immunostaining for nitrotyrosine was evident in the tumor epithelial/endothelial and inflammatory cells. In contrast, only mild immunoreactivity for nitrotyrosine was detected in low and high dose groups (p=0.01 and p=0.002)(Figure 3). Staining for macrophages (CD-68) demonstrated an increase in both the number and the activity of macrophages in PBS-treated tumors (Figure 3). A significant decrease in the macrophage count was found in low and high dose groups (p=0.03 and p=0.01) (Figure 3).

MnTE-2-PyP^{5+} increases tumor oxygenation

PBS-treated tumors exhibited strong HIF-1 α nuclear staining, (Figure 4). In a low dose group, the immunoreactivity of HIF-1α displayed trends towards significant reduction, but was significantly reduced in a high dose group (5 mg/kg, twice daily), (p=0.02) (Figure 4E). Western blot analysis further confirmed the HIF-1α results (Figure 4E). CAIX immunoreactivity (p=0.02 and p=0.006) and pimonidazole staining (p=0.03 and p=0.02) was significantly reduced in both low and high dose groups when compared to PBS group (Figure 4).

MnTE-2-PyP^{5+} decreases the angiogenic profile of tumors

Lower levels of VEGF expression were observed in tumors from mice treated with both low and high dose of MnTE-2-PyP^{5+} than with PBS (p=0.04 and p=0.01) (Figure 5). CD31 also showed a high density of microvessels (MVD) in saline-treated tumors. We observed a decrease in MVD when comparing tumors of mice treated with PBS versus low dose (p=0.06) and it becomes significant when mice were treated with high dose (p-0.02) (Figure 5). When proliferating capillaries index (PCI) was analyzed with CD105 staining (Figure 5), it also displayed a high endothelial proliferation in PBS-treated tumors. We observed a significant decrease in PCI when comparing tumors treated with PBS versus low (p=0.008) or high dose (p=0.03) (Figure 5).

Co-localization of blood vessels with Nox-4 and nitrotyrosine

Representative images of 4T1 tumors stained for CD31 pairing with Nox-4 and nitrotyrosine are shown in Figure 6. Co-localization of Nox-4 and nitrotyrosine with CD31 displayed higher expression in angiogenic areas.

Co-localization of macrophages with Nox-4 and nitrotyrosine

Representative images of 4T1 tumors stained for CD68 pairing with Nox-4 and nitrotyrosine are shown in Figure 7. Co-localization of Nox-4 and nitrotyrosine with CD68 displayed higher expression in inflammatory spots.

MnTE-2-PyP^{5+} does not affect tumor cell proliferation and apoptosis (data not shown)

To demonstrate the tumor proliferative capacity, we counted cells with Ki-67 positive nuclei in random fields for each treatment arm. Quantification confirmed that, compared to PBS, low and high doses did not significantly reduce cell proliferation. We next checked the other side of the proliferation: "apoptosis" balance by labeling cells for activated caspase 3 (aCASP-3), a marker of apoptosis, on slices from treated tumors. Interestingly, these tumors also did not display any difference. Such data also support the notion that the anti-tumor effects are primarily on the levels of endothelial cells.

Discussion

Tumors are under persistent oxidative stress and are thus constantly inflamed [28,35,45–47]. Several studies reported that increased oxidant/antioxidant ratio is directly related to tumor progression, angiogenesis and migration/invasion [35]. Tumor cells produce ROS/RNS at a far greater rate than do the non-transformed cell lines [48]; markers of constitutive oxidative stress have been detected in samples from *in vivo* breast carcinomas [49,50]. 8-Hydroxy-2′-deoxyguanosine, oxidatively modified DNA base product, are almost 10 times more prevalent in invasive ductal breast carcinoma cells than in normal control samples from the same patient [50]. Reactive oxygen and nitrogen species, have a potent stabilizing effects on HIF-1α, and therefore on tumor angiogenesis [18,51–56]. Angiogenesis is critical for tumor growth and invasiveness [57]. Recently, DPI (diphenyleneiodonium chloride, NADPH oxidase inhibitor) and rotenone (inhibitor of complex I of mitochondrial respiration) that decreases levels of endogenous reactive oxygen species, were reported to inhibit angiogenesis and tumor growth [58].

Macrophages are prominent inflammatory cells in tumor tissues, comprising up to 80% of the cell mass in breast carcinoma [59]. They are major producers of ROS/RNS and play an important part in promoting tumor growth and progression [60,61]. Tumor-associated macrophages have been shown to deliver a sublethal oxidative stress to murine mammary carcinoma [62]. Tumor necrosis factor-a secreted by tumor-associated macrophages is shown

to induce cellular oxidative stress [63]. Macrophages are generally at higher levels in more hypoxic tumors as seen in primary human breast carcinomas and in various animal tumors [47,64–67]. In response to low oxygen tension prevalent in tumors, macrophages are recruited from the circulation, where they are activated to undergo the respiratory burst releasing superoxide and nitric oxide [65–68], which affects signaling events that in turn increases leukocyte migration and vascular permeability, tumorgrowth, invasion, metastasis, cytokine production and angiogenesis. We have previously found that if macrophages were co-cultured under hypoxia with MnTE-2-PyP^{5+}, superoxide production was suppressed to baseline levels [69]. Attempts have been made to reduce the number of macrophages in tumors. In a rat model of prostate cancer, anti-angiogenic drugs markedly reduced tumor associated macrophage numbers (<50% of controls), along with tumor growth [70].

Our data show that MnTE-2-PyP^{5+} accumulates in tumor dose dependently; 7.5-fold increase in dose resulted in 6-fold increase in tumor drug level. Data also show that drug in tumors did reach saturation levels, which allows for further enhancement of anti-angiogenesis with increased dosing. Our data further clearly show that tumor oxidative stress was greatly suppressed by MnTE-2-PyP^{5+} in a dose dependent manner. Macrophage infiltration, NADHP oxidase levels, 3-nitrotyrosine formation (an indicator of $ONOO^-$ formation) [71,72] and DNA oxidation were all lowered in tumors in drug-treated groups and most so with high dose of MnTE-2-PyP^{5+} (Figure 3). NADPH oxidases appear to be the major components of tumor oxidative stress [73–76] and Nox-4-generated $O_2^{\cdot -}/H_2O_2$ were shown to stabilize and/or increase expression of HIF-1α [77,78]. Because MnTE-2-PyP^{5+} diminished levels of ROS/RNS, as expected (based on our previous findings [18,40] hypoxia was reduced (pimonidazole), as well as HIF-1α and carbonic anhydrase IX expressions (Figure 4). Consequently the expression of the corresponding VEGF protein was diminished resulting in significant suppression of angiogenesis as observed through decrease in microvessel density and endothelial proliferation (Figure 5). Immunofluorescent immunohistochemistry displayed Nox-4/nitrotyrosine co-localization with angiogenic hot spots in tumor (Figure 6). Co-localization of Nox-4/nitrotyrosine with macrophages was also seen (Figure 7).

When the tumor is small, and existing tumor vasculature can still support its growth, the anti-angiogenic effect of MnTE-2-PyP^{5+} was small, but became significant once the tumor growth accelerates, and new vasculature as well as vasculature remodeling occurs. The latter was accompanied by cycling hypoxia//reoxygenation which further enhances ROS/RNS production (Figure 2). Tumors cease to grow at ~day 14. The pharmacokinetic studies [43] indicate that a loading dose of MnTE-2-PyP^{5+} may be necessary for a certain time period, followed by a maintenance dosing. Further studies will optimize the dosing regime whereby anti-cancer effects may be enhanced. Our data are in agreement with the trend of the tumor growth/suppression observed when NOS inhibitor L-NAME was tested in a same 4T1 murine breast tumor model in Balb/C mice where the tumor suppression effect becomes obvious only after ~15th day.

Two previous studies on 4T1 tumor growth in Balb/C mice utilizing MnTE-2-PyP^{5+} were performed. In a 4T1 window chamber study on BALB/c mice, the very first encouraging data on tumor suppression by MnTE-2-PyP^{5+} were provided although the mechanism of action was at that point still not understood. In that study a CMV-RFP construct was introduced into tumors that allows expression of red fluoresecence protein (RFP) controlled by cytomegalovirus (CMV) promoter so that tumor cells can be tracked. Details are given in ref 18. The 4T1 line also expresses hypoxia responsive green fluorescent protein serving as a reporter for HIF-1α, which allows a serial monitoring of HIF-1 activity levels by intravital fluorescence activity. The data indicate that anti-angiogenic effects became obvious at ~ day 10, and becomes dramatic at 2 weeks after transplantation of tumors on mouse back (Figure 8A) whereupon the tumors become necrotic and start to shrink (Figure 8B and 8C). It was also obvious that

angiogenic suppression by MnTE-2-PyP^{5+} begins early on while the tumors are still similar to the size of the control PBS-treated tumors. Such data are consistent with the finding in this study. In a subsequent (2nd) study [17,18] MnTE-2-PyP was given to BALB/c mouse in 3 doses only, either every 12 hours within first 36 hours [17], or every 24 hours within first 74 hours after tumors reached volume of ~200 mm^3 [18]. At the time of drug administration, tumors had been in a slow initial stage of its growth. The pharmacokinetic study [43] suggests that such drug delivery could not have provided the tumor levels of MnTE-2-PyP^{5+} required throughout its aggressive growth and explains the absence of effects in a second study. However, more recent data keep showing that MnTE-2-PyP prevents significantly-to-fully the activation of major transcription factors [16–18,21,22,24,69] involved in cell proliferation and apoptosis and angiogenesis, and clearly indicate that the very first data should not be overlooked and that there is a rational behind the MnP anti-cancer activity which relates the ROS/RNS scavenging ability of Mn porphyrin directly to the redox-sensitive cellular transcriptional activity. Therefore the cancer research continued and eventually, this 3rd study was performed with a comprehensive insight into tumor angiogenesis and oxidative stress, and with the goal of explaining if and why a catalytic SOD mimic/peroxynitrite scavenger would exert anti-cancer effects. Data for the first time show clearly that MnTE-2-PyP^{5+} has anti-cancer effect in its own right, due at least in part to the suppression of oxidative stress (thus levels of signaling reactive species), which in turn suppresses cellular transcriptional activity and leads to the suppression of tumor vasculature growth. We have not observed a significant effect of MnTE-2-PyP^{5+} on proliferation and apoptosis of tumor cells, per se, which further supports the notion that the major anti-tumor impact occurs on the level of tumor vasculature/endothelial cells [46,79]. Also, Moeller et al [17] and our preliminary experiments on different tumor cell lines including CaCo, 4T1, HCT116, and HeLa (Ye X, Batinic-Haberle, I et al, unpublished) indicate the lack of cytotoxicity of MnTE-2-PyP^{5+} at up to mM levels.

Gao et al recently reported that a stoichiometric antioxidant, *N*-acetylcysteine, exerts anti-tumor effects which are HIF-dependent [80]. Our data support their findings. Therefore, the scavenging of ROS/RNS by antioxidants, which suppresses cellular transcriptional activity, could be an appropriate strategy for anticancer therapy. The catalytical scavengers would be advantageous. The effects may be increased with more cell permeable compounds such as the 4 orders of magnitude more lipophilic hexyl analogue, MnTnHex-2-PyP^{5+}. This analogue has been up to 120-fold more effective in several animal models of oxidative stress injuries [16, 19,25], due predominantly to its enhanced lipohilicity [81]. A 3000-fold enhancement in an oxygen/glucose deprivation neuronal model as a result of increased lipophilicity has also been observed with the octyl analogue, MnTnOct-2-PyP^{5+} when compared to MnTE-2-PyP^{5+} [82]. The anti-cancer effects may further be increased if the drug is combined with radiation and hyperthermia [17,40]. Preliminary data from our group (Ye X et al, unpublished) indicate that Mn porphyrins enhance chemotherapy also.

Conclusions

Our study indicates for the first time that a catalytic scavenger of superoxide and peroxyntrite, MnTE-2-PyP^{5+} has anti-cancer activity in its own right. This effect is the result of the redox-based impact of the drug on the oxidative stress whereby decreased levels of reactive species lead to the suppression of HIF/VEGF pathways and therefore suppression of tumor angiogenesis. Our work has important implication for follow up studies aimed at enhancing tumor therapy *via*: **(1)** exploring the possible enhancement of anti-cancer effect utilizing more bioavailable drugs; **(2)** optimizing drug dosing regimes and **(3)** combining catalytic antioxidants with irradiation, hyperthermia and chemotherapy. Given the additional ability to radioprotect normal tissue and its potential in maintaining analgesic effects when morphine is given chronically, MnTE-2-PyP^{5+} can exert triple action in cancer treatment, being therefore advantageous over other anti-cancer drugs.

Acknowledgments

We are grateful to Irwin Fridovich for critical reading of the manuscript. I.B.H. acknowledges the support by DOD CDMRP (BC024326) and the National Institutes of Health grant U19AI67798-01, and Wallace H Coulter Translational Partners Grant Programs. I.S. is thankful for the support of NIH/NCI Duke Comprehensive Cancer Center Core Grant (5-P30-CA14236-33), Z.R. to NIH-5U19-AI-067798-04, and Z.V. to RO1 CA 098452.

Abbreviations

SOD
: superoxide dismutase

MnP
: any porphyrin

$Mn^{III}P/Mn^{II}P$
: oxidized(III)/reduced(II) porphyrin at Mn site

MnTE-2-PyP^{5+}
: Mn(III) *meso*-tetrakis(*N*-ethylpyridinium-2-yl)porphyrin (AEOL10113)

MnTnHex-2-PyP^{5+}
: Mn(III) *meso*-tetrakis(*N*-n-hexylpyridinium-2-yl)porphyrin

MnTnOct-2-PyP^{5+}
: Mn(III) *meso*-tetrakis (*N*-n-octylpyridinium-2-yl)porphyrin

MnTDE-2-ImP^{5+}
: Mn(III) meso-tetrakis (2-diethylimidazolium)porphyrin (AEOL10150)

HIF-1α
: hypoxia inducible factor-1α

NF-κB
: nuclear factor κB

AP-1
: activator protein-1

CD31
: marker for microvessel density

CD105
: marker for proliferative capillary index

CD68
: marker of macrophage infiltration

CAIX
: carbonic anhydrase IX

Nox-4
: homologue of $gp91^{phox}$ catalytic subunit of phagocyte NAD(P)H oxidase

8-OHdG
: 8-hydroxy-2′-deoxyguanosine

DPI
: diphenyleneiodonium chloride

References

1. Batinic-Haberle I, Benov L, Spasojevic I, Fridovich I. The ortho effect makes manganese(III) meso-tetrakis(N-methylpyridinium-2-yl)porphyrin a powerful and potentially useful superoxide dismutase mimic. The Journal of biological chemistry 1998;273:24521–24528. [PubMed: 9733746]
2. Batinic-Haberle I, Spasojevic I, Hambright P, Benov L, Crumbliss AL, Fridovich I. Relationship among Redox Potentials, Proton Dissociation Constants of Pyrrolic Nitrogens, and in Vivo and in Vitro Superoxide Dismutating Activities of Manganese(III) and Iron(III) Water-Soluble Porphyrins. Inorg Chem 1999;38:4011–4022.
3. Batinic-Haberle I, Spasojevic I, Stevens RD, Bondurant B, Okado-Matsumoto A, Fridovich I, Vujaskovic Z, Dewhirst MW. New PEG-ylated Mn(III) porphyrins approaching catalytic activity of SOD enzyme. Dalton Trans 2006:617–624. [PubMed: 16402149]
4. Batinic-Haberle I, Spasojevic I, Stevens RD, Hambright P, Fridovich I. Manganese(III) Meso Tetrakis Ortho N-alkylpyridylporphyrins. Synthesis, Characterization and Catalysis of O2.− Dismutation . Dalton Trans 2002:2689–2696.
5. Batinic-Haberle I, Spasojevic I, Stevens RD, Hambright P, Neta P, Okado-Matsumoto A, Fridovich I. New class of potent catalysts of O2.− dismutation. Mn(III) ortho-methoxyethylpyridyl- and di-ortho-methoxyethylimidazolylporphyrins. Dalton Trans 2004:1696–1702. [PubMed: 15252564]
6. Reboucas JS, DeFreitas-Silva G, Spasojevic I, Idemori YM, Benov L, Batinic-Haberle I. Impact of electrostatics in redox modulation of oxidative stress by Mn porphyrins: protection of SOD-deficient Escherichia coli via alternative mechanism where Mn porphyrin acts as a Mn carrier. Free radical biology & medicine 2008;45:201–210. [PubMed: 18457677]
7. Spasojevic I, Batinic-Haberle I, Reboucas JS, Idemori YM, Fridovich I. Electrostatic contribution in the catalysis of O2*− dismutation by superoxide dismutase mimics. MnIIITE-2-PyP5+ versus MnIIIBr8T-2-PyP+ The Journal of biological chemistry 2003;278:6831–6837. [PubMed: 12475974]
8. Reboucas JS, Spasojevic I, Tjahjono DH, Richaud A, Mendez F, Benov L, Batinic-Haberle I. Redox modulation of oxidative stress by Mn porphyrin-based therapeutics: the effect of charge distribution. Dalton Trans 2008:1233–1242. [PubMed: 18283384]
9. Ferrer-Sueta G, Batinic-Haberle I, Spasojevic I, Fridovich I, Radi R. Catalytic scavenging of peroxynitrite by isomeric Mn(III) N-methylpyridylporphyrins in the presence of reductants. Chemical research in toxicology 1999;12:442–449. [PubMed: 10328755]
10. Ferrer-Sueta G, Vitturi D, Batinic-Haberle I, Fridovich I, Goldstein S, Czapski G, Radi R. Reactions of manganese porphyrins with peroxynitrite and carbonate radical anion. The Journal of biological chemistry 2003;278:27432–27438. [PubMed: 12700236]
11. DeFreitas-Silva G, Reboucas JS, Spasojevic I, Benov L, Idemori YM, Batinic-Haberle I. SOD-like activity of Mn(II) beta-octabromo-meso-tetrakis(N-methylpyridinium-3-yl)porphyrin equals that of the enzyme itself. Archives of biochemistry and biophysics 2008;477:105–112. [PubMed: 18477465]
12. Batinic-Haberle I, Spasojevic I, Fridovich I. Tetrahydrobiopterin rapidly reduces the SOD mimic Mn (III) ortho-tetrakis(N-ethylpyridinium-2-yl)porphyrin. Free radical biology & medicine 2004;37:367–374. [PubMed: 15223070]
13. Benov L, Batinic-Haberle I, Spasojevic I, Fridovich I. Isomeric N-alkylpyridylporphyrins and their Zn(II) complexes: inactive as SOD mimics but powerful photosensitizers. Archives of biochemistry and biophysics 2002;402:159–165. [PubMed: 12051659]
14. Bottino R, Balamurugan AN, Tse H, Thirunavukkarasu C, Ge X, Profozich J, Milton M, Ziegenfuss A, Trucco M, Piganelli JD. Response of human islets to isolation stress and the effect of antioxidant treatment. Diabetes 2004;53:2559–2568. [PubMed: 15448084]
15. Cernanec JM, Weinberg JB, Batinic-Haberle I, Guilak F, Fermor B. Influence of oxygen tension on interleukin 1-induced peroxynitrite formation and matrix turnover in articular cartilage. The Journal of rheumatology 2007;34:401–407. [PubMed: 17295437]
16. Gauter-Fleckenstein B, Fleckenstein K, Owzar K, Jiang C, Batinic-Haberle I, Vujaskovic Z. Comparison of two Mn porphyrin-based mimics of superoxide dismutase in pulmonary radioprotection. Free radical biology & medicine 2008;44:982–989. [PubMed: 18082148]

17. Moeller BJ, Batinic-Haberle I, Spasojevic I, Rabbani ZN, Anscher MS, Vujaskovic Z, Dewhirst MW. A manganese porphyrin superoxide dismutase mimetic enhances tumor radioresponsiveness. International journal of radiation oncology, biology, physics 2005;63:545–552.

18. Moeller BJ, Cao Y, Li CY, Dewhirst MW. Radiation activates HIF-1 to regulate vascular radiosensitivity in tumors: role of reoxygenation, free radicals, and stress granules. Cancer cell 2004;5:429–441. [PubMed: 15144951]

19. Saba H, Batinic-Haberle I, Munusamy S, Mitchell T, Lichti C, Megyesi J, MacMillan-Crow LA. Manganese porphyrin reduces renal injury and mitochondrial damage during ischemia/reperfusion. Free radical biology & medicine 2007;42:1571–1578. [PubMed: 17448904]

20. Sompol P, Ittarat W, Tangpong J, Chen Y, Doubinskaia I, Batinic-Haberle I, Abdul HM, Butterfield DA, St Clair DK. A neuronal model of Alzheimer's disease: an insight into the mechanisms of oxidative stress-mediated mitochondrial injury. Neuroscience 2008;153:120–130. [PubMed: 18353561]

21. Tse HM, Milton MJ, Piganelli JD. Mechanistic analysis of the immunomodulatory effects of a catalytic antioxidant on antigen-presenting cells: implication for their use in targeting oxidation-reduction reactions in innate immunity. Free radical biology & medicine 2004;36:233–247. [PubMed: 14744635]

22. Zhao Y, Chaiswing L, Oberley TD, Batinic-Haberle I, St Clair W, Epstein CJ, St Clair D. A mechanism-based antioxidant approach for the reduction of skin carcinogenesis. Cancer research 2005;65:1401–1405. [PubMed: 15735027]

23. Rabbani ZN, Batinic-Haberle I, Anscher MS, Huang J, Day BJ, Alexander E, Dewhirst MW, Vujaskovic Z. Long-term administration of a small molecular weight catalytic metalloporphyrin antioxidant, AEOL 10150, protects lungs from radiation-induced injury. International journal of radiation oncology, biology, physics 2007;67:573–580.

24. Rabbani ZN, Salahuddin FK, Yarmolenko P, Batinic-Haberle I, Thrasher B, Gauter-Fleckenstein B, Anscher MS, Dewhirst MW, Vujaskovic Z. Low molecular weight catalytic metalloporphyrin antioxidant AEOL 10150 protects lungs from fractionated radiation. Free radical research. 2007In Press

25. Batinic-Haberle I, Ndengele MM, Cuzzocrea S, Reboucas JS, Masini E, Spasojevic I, Salvemini D. Lipophilicity is a critical parameter that dominates the efficacy of metalloporphyrins in blocking morphine tolerance through peroxynitrite-mediated pathways. Free Radic Biol Med. 2008In press

26. Li F, Sonveaux P, Rabbani ZN, Liu S, Yan B, Huang Q, Vujaskovic Z, Dewhirst MW, Li CY. Regulation of HIF-1alpha stability through S-nitrosylation. Molecular cell 2007;26:63–74. [PubMed: 17434127]

27. Gridley DS, Makinde AY, Luo X, Rizvi A, Crapo JD, Dewhirst MW, Moeller BJ, Pearlstein RD, Slater JM. Radiation and a metalloporphyrin radioprotectant in a mouse prostate tumor model. Anticancer research 2007;27:3101–3109. [PubMed: 17970050]

28. Schafer FQ, Buettner GR. Redox environment of the cell as viewed through the redox state of the glutathione disulfide/glutathione couple. Free radical biology & medicine 2001;30:1191–1212. [PubMed: 11368918]

29. Moeller BJ, Richardson RA, Dewhirst MW. Hypoxia and radiotherapy: opportunities for improved outcomes in cancer treatment. Cancer metastasis reviews 2007;26:241–248. [PubMed: 17440683]

30. Wang M, Kirk JS, Venkataraman S, Domann FE, Zhang HJ, Schafer FQ, Flanagan SW, Weydert CJ, Spitz DR, Buettner GR, Oberley LW. Manganese superoxide dismutase suppresses hypoxic induction of hypoxia-inducible factor-1alpha and vascular endothelial growth factor. Oncogene 2005;24:8154–8166. [PubMed: 16170370]

31. Venkataraman S, Jiang X, Weydert C, Zhang Y, Zhang HJ, Goswami PC, Ritchie JM, Oberley LW, Buettner GR. Manganese superoxide dismutase overexpression inhibits the growth of androgen-independent prostate cancer cells. Oncogene 2005;24:77–89. [PubMed: 15543233]

32. Connor KM, Hempel N, Nelson KK, Dabiri G, Gamarra A, Belarmino J, Van De Water L, Mian BM, Melendez JA. Manganese superoxide dismutase enhances the invasive and migratory activity of tumor cells. Cancer research 2007;67:10260–10267. [PubMed: 17974967]

33. Dasgupta J, Subbaram S, Connor KM, Rodriguez AM, Tirosh O, Beckman JS, Jourd'Heuil D, Melendez JA. Manganese superoxide dismutase protects from TNF-alpha-induced apoptosis by

increasing the steady-state production of H2O2. Antioxidants & redox signaling 2006;8:1295–1305. [PubMed: 16910777]

34. Venkataraman S, Wagner BA, Jiang X, Wang HP, Schafer FQ, Ritchie JM, Patrick BC, Oberley LW, Buettner GR. Overexpression of manganese superoxide dismutase promotes the survival of prostate cancer cells exposed to hyperthermia. Free radical research 2004;38:1119–1132. [PubMed: 15512801]
35. Hempel N, Ye H, Abessi B, Mian B, Melendez JA. Altered redox status accompanies progression to metastatic human bladder cancer. Free radical biology & medicine. 2008
36. Kinnula VL, Crapo JD. Superoxide dismutases in malignant cells and human tumors. Free radical biology & medicine 2004;36:718–744. [PubMed: 14990352]
37. Mocellin S, Bronte V, Nitti D. Nitric oxide, a double edged sword in cancer biology: searching for therapeutic opportunities. Medicinal research reviews 2007;27:317–352. [PubMed: 16991100]
38. Ray A, Chakraborti A, Gulati K. Current trends in nitric oxide research. Cellular and molecular biology (Noisy-le-Grand, France) 2007;53:3–14.
39. Jackson IL, Batinic-Haberle I, Sonveaux P, Dewhirst MW, Vujaskovic Z. ROS production and angiogenic regulation by macrophages in response to heat therapy. Int J Hyperthermia 2006;22:263–273. [PubMed: 16754348]
40. Jackson IL, Gaunter-Fleckenstein BM, Batinic-Haberle I, Poulton S, Zhao Y, Dewhirst MW, Vujaskovic Z. Hyperthermia enhances the anti-angiogenic effect of metalloporphyrin mimetic of superoxide dismutase. 24th Annual Meeting of the European Society for Hyperthermic Oncology, Prague, Czech Republic. 2007
41. Bradford MM. A rapid and sensitive method for the quantitation of microgram quantities of protein utilizing the principle of protein-dye binding. Anal Biochem 1976;72:248–254. [PubMed: 942051]
42. Zhang X, Lee TH, Davidson C, Lazarus C, Wetsel WC, Ellinwood EH. Reversal of cocaine-induced behavioral sensitization and associated phosphorylation of the NR2B and GluR1 subunits of the NMDA and AMPA receptors. Neuropsychopharmacology 2007;32:377–387. [PubMed: 16794574]
43. Spasojevic I, Chen Y, Noel TJ, Fan P, Zhang L, Reboucas JS, St Clair DK, Batinic-Haberle I. Pharmacokinetics of the potent redox-modulating manganese porphyrin, MnTE-2-PyP(5+), in plasma and major organs of B6C3F1 mice. Free radical biology & medicine 2008;45:943–949. [PubMed: 18598757]
44. Spasojevic I, Chen Y, Noel TJ, Yu Y, Cole MP, Zhang L, Zhao Y, St Clair DK, Batinic-Haberle I. Mn porphyrin-based superoxide dismutase (SOD) mimic, MnIIITE-2-PyP5+, targets mouse heart mitochondria. Free radical biology & medicine 2007;42:1193–1200. [PubMed: 17382200]
45. Brown NS, Bicknell R. Hypoxia and oxidative stress in breast cancer. Oxidative stress: its effects on the growth, metastatic potential and response to therapy of breast cancer. Breast Cancer Res 2001;3:323–327. [PubMed: 11597322]
46. Dewhirst MW, Cao Y, Moeller B. Cycling hypoxia and free radicals regulate angiogenesis and radiotherapy response. Nature reviews 2008;8:425–437.
47. Hussain SP, Harris CC. Inflammation and cancer: an ancient link with novel potentials. International journal of cancer 2007;121:2373–2380.
48. Wiseman H, Halliwell B. Damage to DNA by reactive oxygen and nitrogen species: role in inflammatory disease and progression to cancer. The Biochemical journal 1996;313:17 –29. [PubMed: 8546679]
49. Portakal O, Ozkaya O, Erden Inal M, Bozan B, Kosan M, Sayek I. Coenzyme Q10 concentrations and antioxidant status in tissues of breast cancer patients. Clin Biochem 2000;33:279–284. [PubMed: 10936586]
50. Toyokuni S, Okamoto K, Yodoi J, Hiai H. Persistent oxidative stress in cancer. FEBS letters 1995;358:1 –3. [PubMed: 7821417]
51. Brune B, Zhou J. The role of nitric oxide (NO) in stability regulation of hypoxia inducible factor-1alpha (HIF-1alpha). Current medicinal chemistry 2003;10:845–855. [PubMed: 12678687]
52. Brune B, Zhou J, von Knethen A. Nitric oxide, oxidative stress, and apoptosis. Kidney international 2003:S22–24. [PubMed: 12694301]

53. Chandel NS, Maltepe E, Goldwasser E, Mathieu CE, Simon MC, Schumacker PT. Mitochondrial reactive oxygen species trigger hypoxia-induced transcription. Proceedings of the National Academy of Sciences of the United States of America 1998;95:11715–11720. [PubMed: 9751731]
54. Chandel NS, McClintock DS, Feliciano CE, Wood TM, Melendez JA, Rodriguez AM, Schumacker PT. Reactive oxygen species generated at mitochondrial complex III stabilize hypoxia-inducible factor-1alpha during hypoxia: a mechanism of O2 sensing. The Journal of biological chemistry 2000;275:25130–25138. [PubMed: 10833514]
55. Gao N, Ding M, Zheng JZ, Zhang Z, Leonard SS, Liu KJ, Shi X, Jiang BH. Vanadate-induced expression of hypoxia-inducible factor 1 alpha and vascular endothelial growth factor through phosphatidylinositol 3-kinase/Akt pathway and reactive oxygen species. The Journal of biological chemistry 2002;277:31963–31971. [PubMed: 12070140]
56. Haddad JJ, Land SC. A non-hypoxic, ROS-sensitive pathway mediates TNF-alpha-dependent regulation of HIF-1alpha. FEBS letters 2001;505:269–274. [PubMed: 11566189]
57. Folkman J. Tumor angiogenesis: therapeutic implications. The New England journal of medicine 1971;285:1182–1186. [PubMed: 4938153]
58. Xia C, Meng Q, Liu LZ, Rojanasakul Y, Wang XR, Jiang BH. Reactive oxygen species regulate angiogenesis and tumor growth through vascular endothelial growth factor. Cancer research 2007;67:10823–10830. [PubMed: 18006827]
59. Bingle L, Brown NJ, Lewis CE. The role of tumour-associated macrophages in tumour progression: implications for new anticancer therapies. The Journal of pathology 2002;196:254–265. [PubMed: 11857487]
60. Lamagna C, Aurrand-Lions M, Imhof BA. Dual role of macrophages in tumor growth and angiogenesis. J Leukoc Biol 2006;80:705–713. [PubMed: 16864600]
61. Leek RD, Harris AL. Tumor-associated macrophages in breast cancer. Journal of mammary gland biology and neoplasia 2002;7:177–189. [PubMed: 12463738]
62. Kundu N, Zhang S, Fulton AM. Sublethal oxidative stress inhibits tumor cell adhesion and enhances experimental metastasis of murine mammary carcinoma. Clin Exp Metastasis 1995;13:16 –22. [PubMed: 7820952]
63. Fulton AM, Chong YC. The role of macrophage-derived TNFalpha in the induction of sublethal tumor cell DNA damage. Carcinogenesis 1992;13:77 –81. [PubMed: 1733575]
64. Knowles H, Leek R, Harris AL. Macrophage infiltration and angiogenesis in human malignancy. Novartis Foundation symposium 256:189–200. [PubMed: 15027491]discussion 200–184, 259–169; 2004.
65. Lewis C, Murdoch C. Macrophage responses to hypoxia: implications for tumor progression and anti-cancer therapies. The American journal of pathology 2005;167:627–635. [PubMed: 16127144]
66. Lewis CE, Hughes R. Inflammation and breast cancer. Microenvironmental factors regulating macrophage function in breast tumours: hypoxia and angiopoietin-2. Breast Cancer Res 2007;9:209. [PubMed: 17601353]
67. Talks KL, Turley H, Gatter KC, Maxwell PH, Pugh CW, Ratcliffe PJ, Harris AL. The Expression and Distribution of the Hypoxia-Inducible Factors HIF-1{alpha} and HIF-2{alpha} in Normal Human Tissues, Cancers, and Tumor-Associated Macrophages. The American journal of pathology 2000;157:411–421. [PubMed: 10934146]
68. Larsen M, Tazzyman S, Lund EL, Junker N, Lewis CE, Kristjansen PE, Murdoch C. Hypoxia-induced secretion of macrophage migration-inhibitory factor from MCF-7 breast cancer cells is regulated in a hypoxia-inducible factor-independent manner. Cancer letters 2008;265:239–249. [PubMed: 18353538]
69. Jackson IL, Chen L, Batinic-Haberle I, Vujaskovic Z. Superoxide dismutase mimetic reduces hypoxia-induced O2*−, TGF-beta, and VEGF production by macrophages. Free radical research 2007;41:8–14. [PubMed: 17164174]
70. Joseph IB, Isaacs JT. Macrophage role in the anti-prostate cancer response to one class of antiangiogenic agents. Journal of the National Cancer Institute 1998;90:1648–1653. [PubMed: 9811314]

71. Bartesaghi S, Ferrer-Sueta G, Peluffo G, Valez V, Zhang H, Kalyanaraman B, Radi R. Protein tyrosine nitration in hydrophilic and hydrophobic environments. Amino acids 2007;32:501–515. [PubMed: 17077966]
72. Szabo C, Ischiropoulos H, Radi R. Peroxynitrite: biochemistry, pathophysiology and development of therapeutics. Nat Rev Drug Discov 2007;6:662–680. [PubMed: 17667957]
73. Brar SS, Corbin Z, Kennedy TP, Hemendinger R, Thornton L, Bommarius B, Arnold RS, Whorton AR, Sturrock AB, Huecksteadt TP, Quinn MT, Krenitsky K, Ardie KG, Lambeth JD, Hoidal JR. NOX5 NAD(P)H oxidase regulates growth and apoptosis in DU 145 prostate cancer cells. American journal of physiology 2003;285:C353–369. [PubMed: 12686516]
74. Brar SS, Kennedy TP, Quinn M, Hoidal JR. Redox signaling of NF-kappaB by membrane NAD(P)H oxidases in normal and malignant cells. Protoplasma 2003;221:117–127. [PubMed: 12768349]
75. Brar SS, Kennedy TP, Sturrock AB, Huecksteadt TP, Quinn MT, Whorton AR, Hoidal JR. An NAD(P)H oxidase regulates growth and transcription in melanoma cells. American journal of physiology 2002;282:C1212–1224. [PubMed: 11997235]
76. Lim SD, Sun C, Lambeth JD, Marshall F, Amin M, Chung L, Petros JA, Arnold RS. Increased Nox1 and hydrogen peroxide in prostate cancer. The Prostate 2005;62:200–207. [PubMed: 15389790]
77. Maranchie JK, Zhan Y. Nox4 is critical for hypoxia-inducible factor 2-alpha transcriptional activity in von Hippel-Lindau-deficient renal cell carcinoma. Cancer research 2005;65:9190–9193. [PubMed: 16230378]
78. Simon MC. Mitochondrial reactive oxygen species are required for hypoxic HIF alpha stabilization. Advances in experimental medicine and biology 2006;588:165–170. [PubMed: 17089888]
79. Dewhirst MW, Richardson R, Cardenas-Navia I, Cao Y. The relationship between the tumor physiologic microenvironment and angiogenesis. Hematology/oncology clinics of North America 2004;18:973–990. [PubMed: 15474330]
80. Gao P, Zhang H, Dinavahi R, Li F, Xiang Y, Raman V, Bhujwalla ZM, Felsher DW, Cheng L, Pevsner J, Lee LA, Semenza GL, Dang CV. HIF-dependent antitumorigenic effect of antioxidants in vivo. Cancer cell 2007;12:230–238. [PubMed: 17785204]
81. Kos I, Reboucas JS, DeFreitas-Silva G, Vujaskovic Z, Dewhirst MW, Spasojevic IIB-H. The effect of lipophilicity of porphyrin-based antioxidants. Comparison of ortho and meta isomers of Mn(III) N-alkylpyridylporphyrins. Free radical biology & medicine 2009;47:72–78. [PubMed: 19361553]
82. Wise-Faberowski L, Warner DS, Spasojevic I, Batinic-Haberle I. The effect of lipophilicity of Mn(III) ortho N-alkylpyridyl- and diortho N, N′-imidazolylporphyrins in two in-vitro models of oxygen and glucose deprivation-induced neuronal death. Free radical research 2009;43:329–339. [PubMed: 19259881]

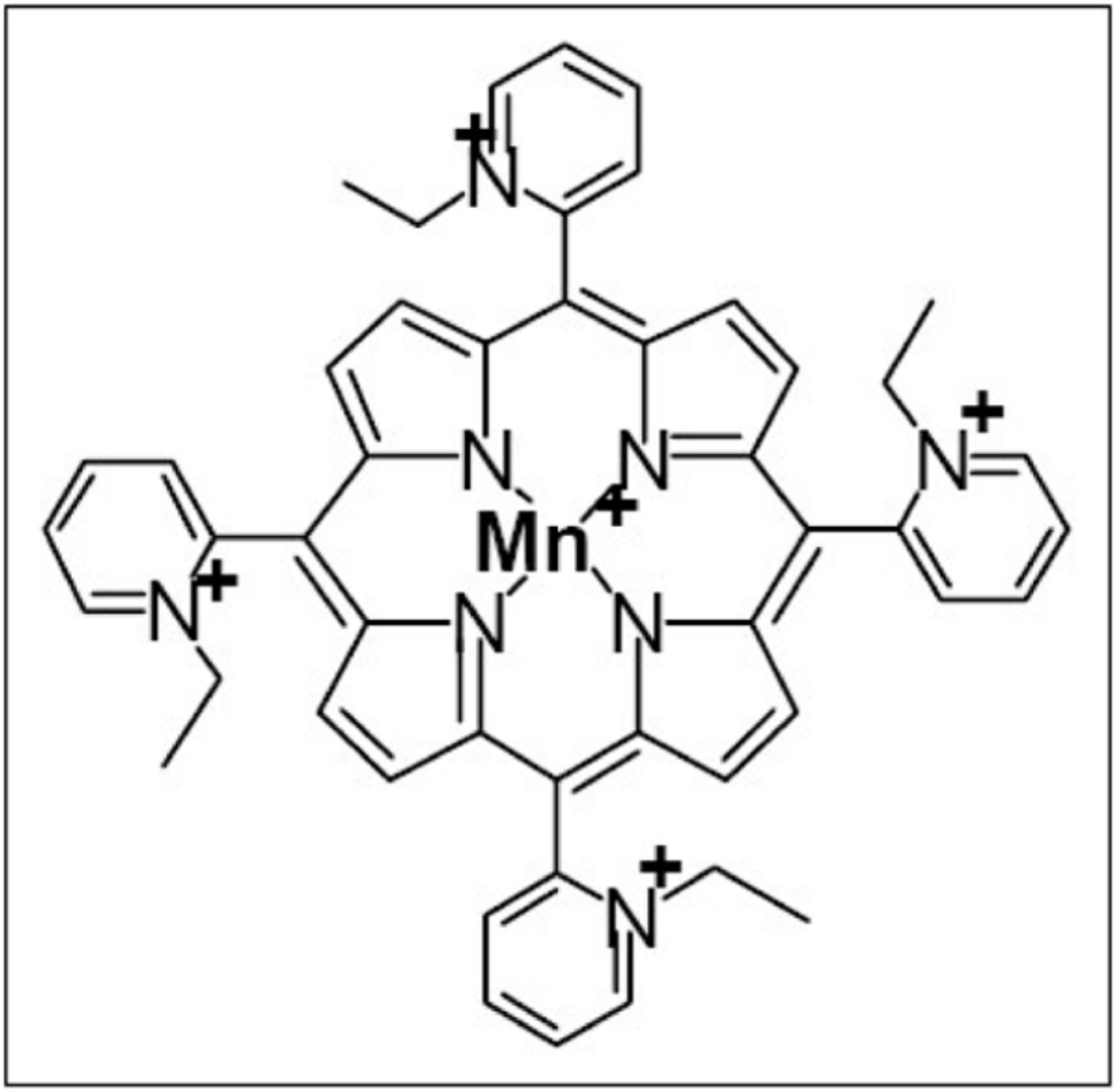

Figure 1.
Structure of MnTE-2-PyP^{5+}

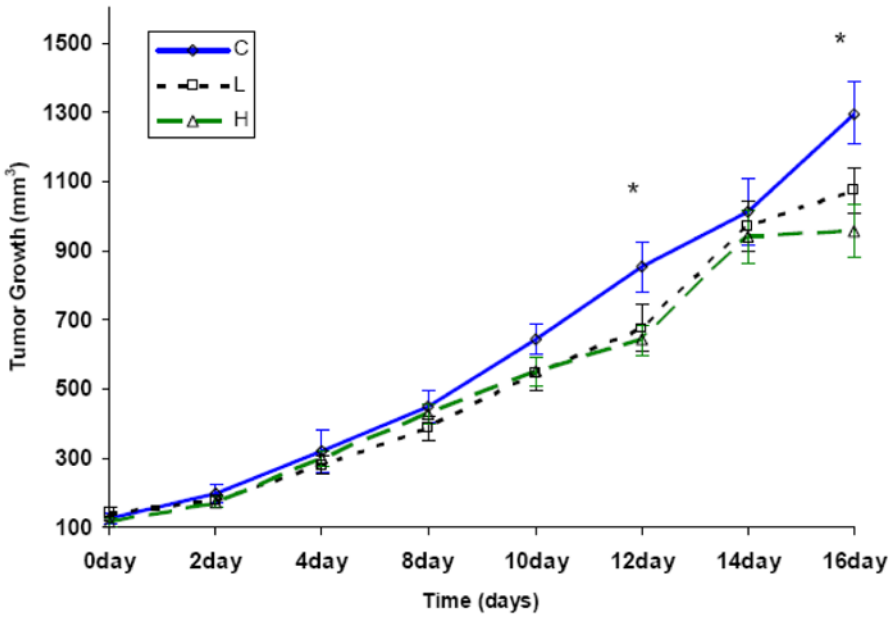

Figure 2. Anticancer activity of Mn(III) tetrakis(*N*-ethylpyridinium-2-yl) porphyrin (MnTE-2-PyP^{5+}

4T1 murine breast tumors were grown in Balb/C mice, allowed to reach ≥200 mm^3 in size, and randomized to one of three treatment groups: (*1*) phosphate-buffered saline (PBS, control), (*2*) MnTE-2-PyP^{5+} (2mg/kg/day given in two daily increments), (*3*) MnTE-2-PyP^{5+} (15 mg/kg/day given in two daily increments). The high dose-treatment group had significant effects on tumor growth delay starting at day 12, as compared to control (n = 25 per group)(*$p < 0.02$ vs. Control).

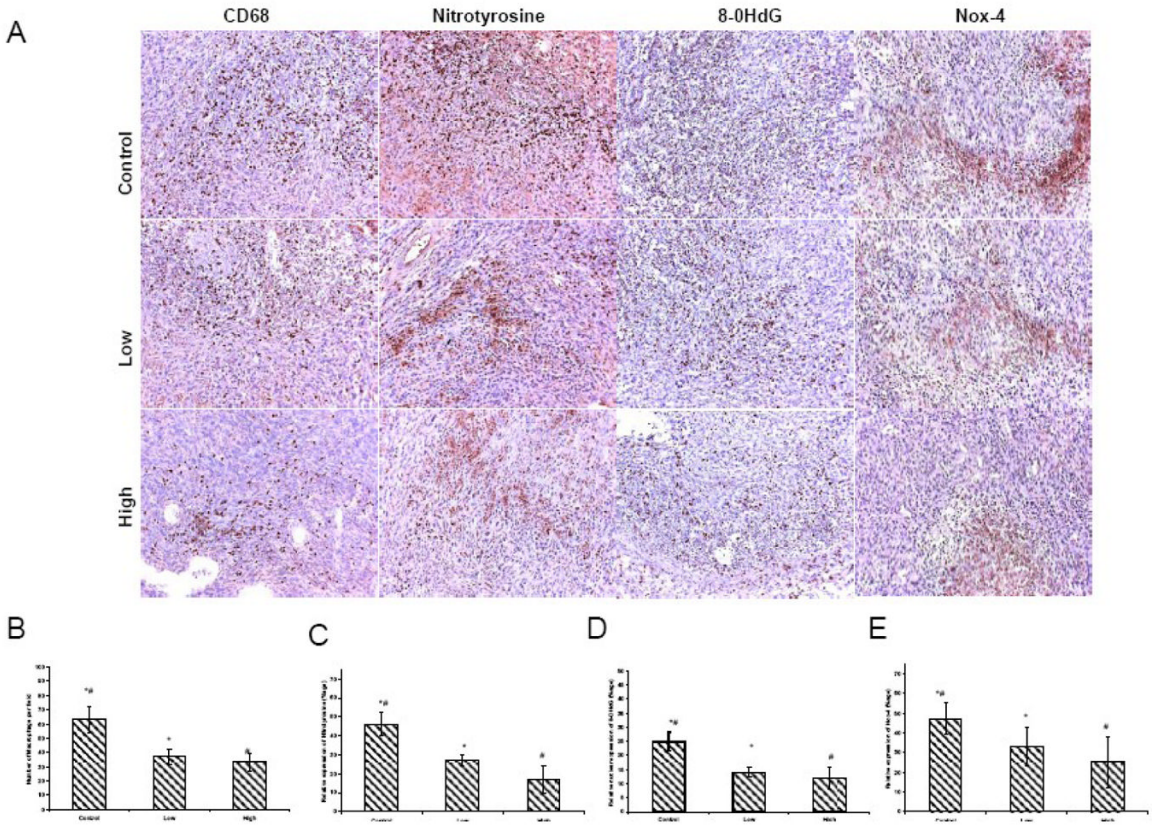

Figure 3. (A)Immunohistochemistry of Nox-4, 8-OHdG, 3-Nitrotyrosine and CD68

The tumors treated with low and high dose of MnTE-2-PyP^{5+} exhibited much fewer activated macrophages and lower level of oxidative stress. These photomicrographs are representative of results obtained from 5–6 animals in each group. **(B).** Semiquantitative anlysis for Nox-4 displayed an intense expression in control tumors. A significant decrease in the Nox-4 was found in the groups receiving MnTE-2-PyP^{5+} treatment compared with the control alone. **(C).** PBS-treated tumor sections displayed strong immunoreactivity for the presence of 3-nitrotyrosine. Significantly reduced immunoreactivity was detected in MnTE-2-PyP^{5+} treated groups. **(D).** 8-OHdG expression revealed strong nuclear oxidation in control tumors. A significant reduction in DNA oxidation was found with MnTE-2-PyP^{5+} treatment. **(E).** Semiquantitative anlysis for macrophages demonstrated an increase in number of macrophages in control tumors. A significant decrease in the macrophage count was found in the groups receiving MnTE-2-PyP^{5+} treatment compared with the PBS group.

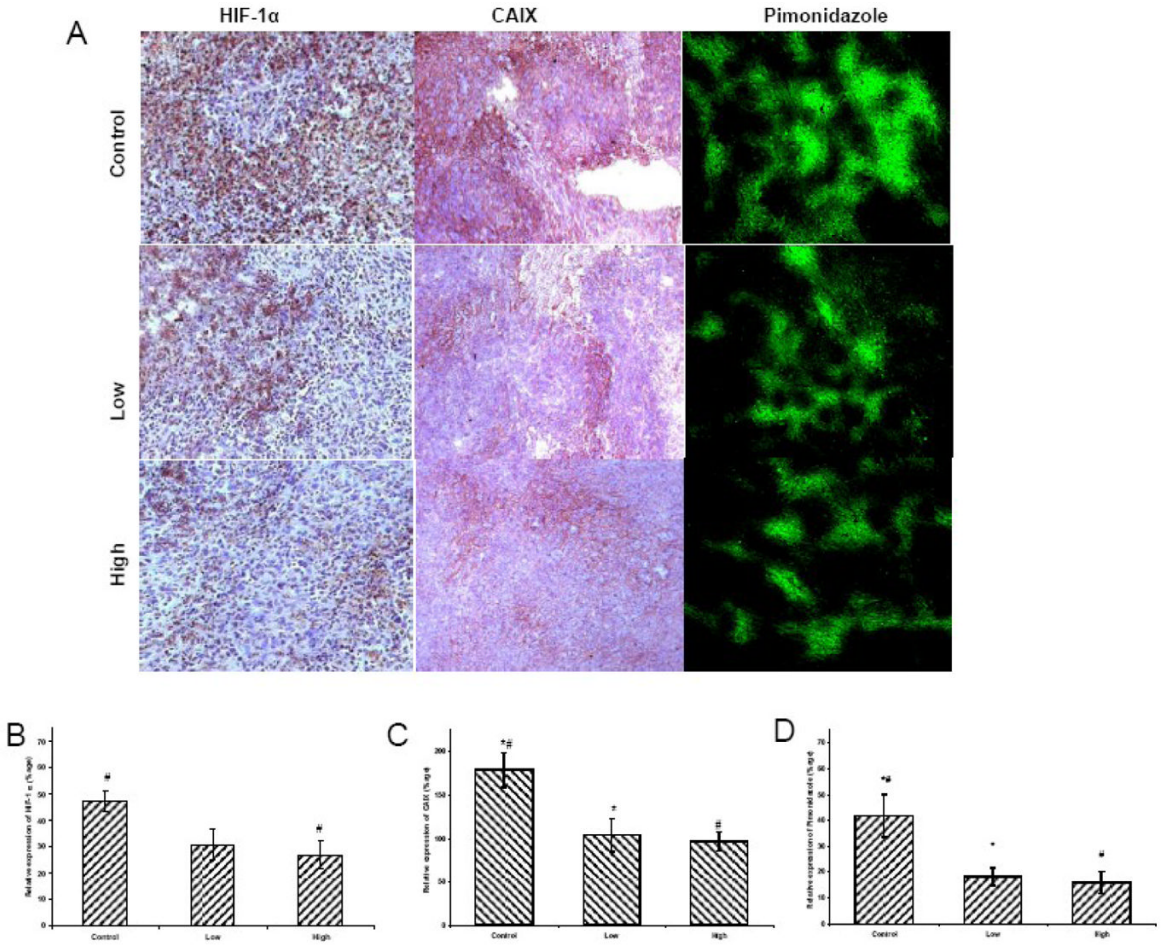

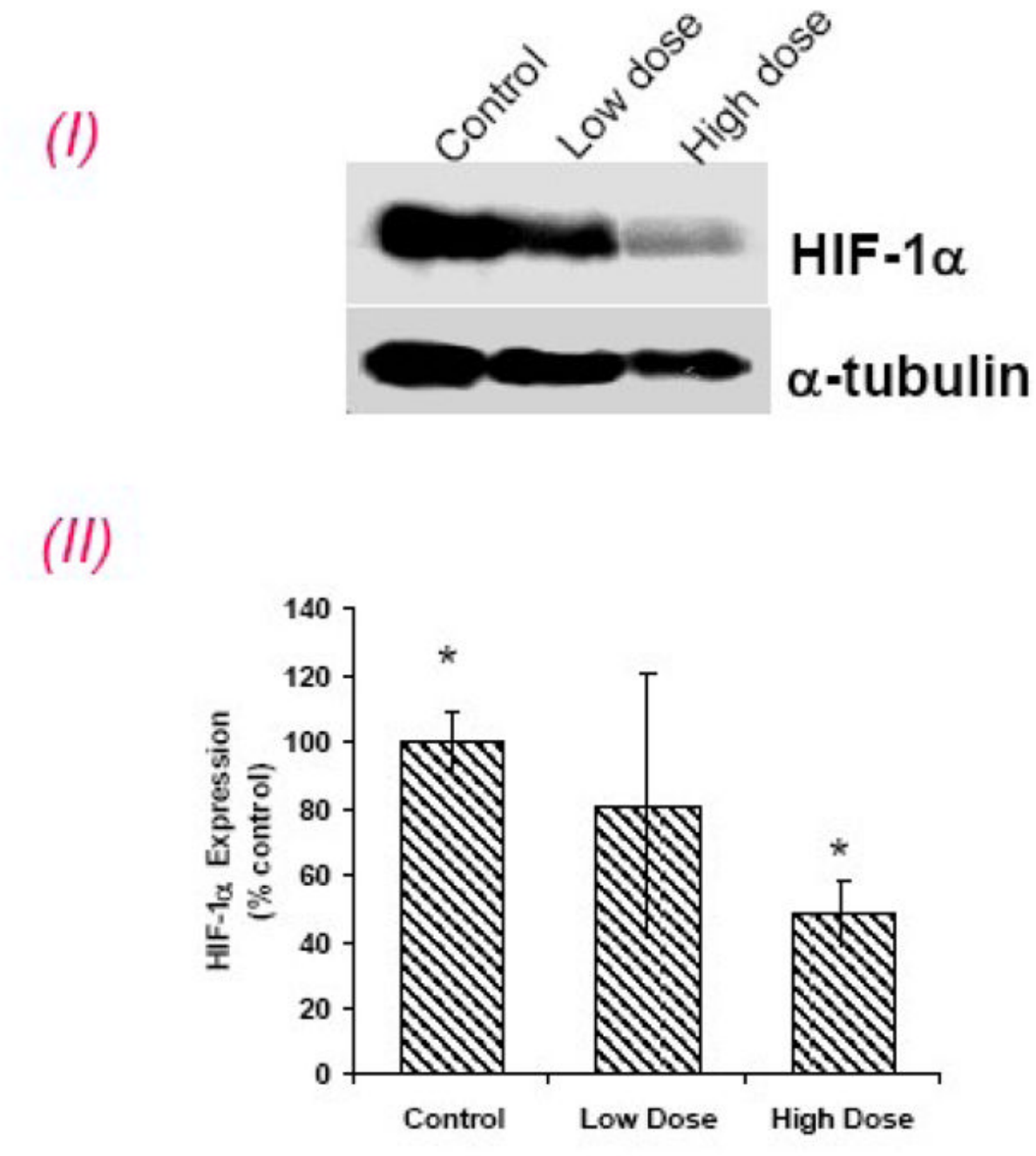

Figure 4. (A)Immunohistochemistry of HIF-1 α, CAIX, and pimonidazole

HIF-1α, positive nuclear staining (brown) was most intense in control tumors, less so in the low- and significantly less in high dose treatment groups. CA IX and pimonidazole were significantly lowered in low and high treatment groups. These photomicrographs are representative of results obtained from five to six animals in each group. Semi-quantitative analysis of **(B)** HIF-1α, **(C)** CAIX and **(D)** pimonidazole.

(E) HIF-1α western blot expression: *(I)*, Representative Western blots for HIF-1α and α-tubulin. *(II)* densitometric readings (HIF-1α/α-tubulin) of the Western blot expressed as percent control (control set to 100%). High dose group significantly inhibited HIF-1α expression. **p* < 0.05.

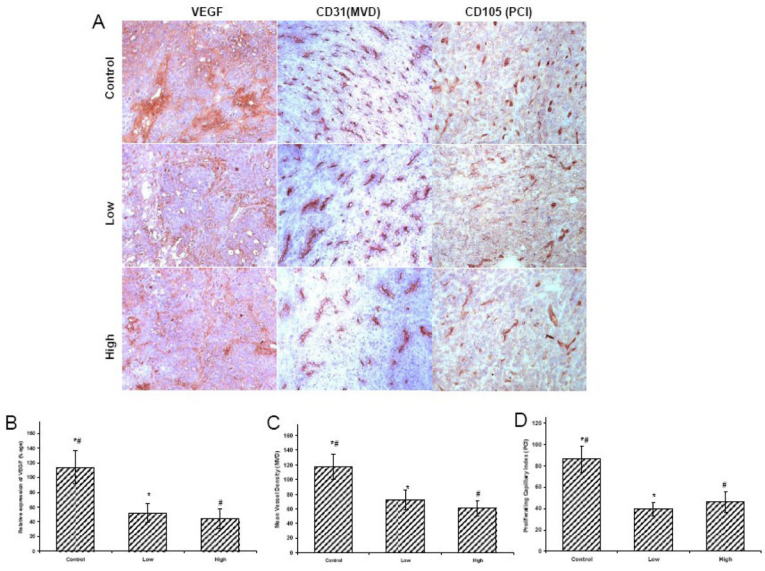

Figure 5. (A)Immunohistochemistry of VEGF, CD31 and CD105

Effect of MnTE-2-PyP^{5+} on angiogenic profile of 4T1 tumors. For VEGF, positive staining (brown) was most intense in control tumors with increased MVD and PCI. However, VEGF expression was significantly lowered after treatment with MnTE-2-PyP^{5+}, compared to control tumors. Similarly less number of blood vessels (MVD) and endothelial proliferation (PCI) were documented in groups treated with MnTE-2-PyP^{5+}. These photomicrographs are representative of results obtained from five to six animals in each group. Semiquantitative analysis of **(B)** VEGF **(C)** Microvessel Density (MVD) **(D)** Proliferating Capillary Index (PCI) in the tumors with or without MnTE-2-PyP^{5+} treatment.

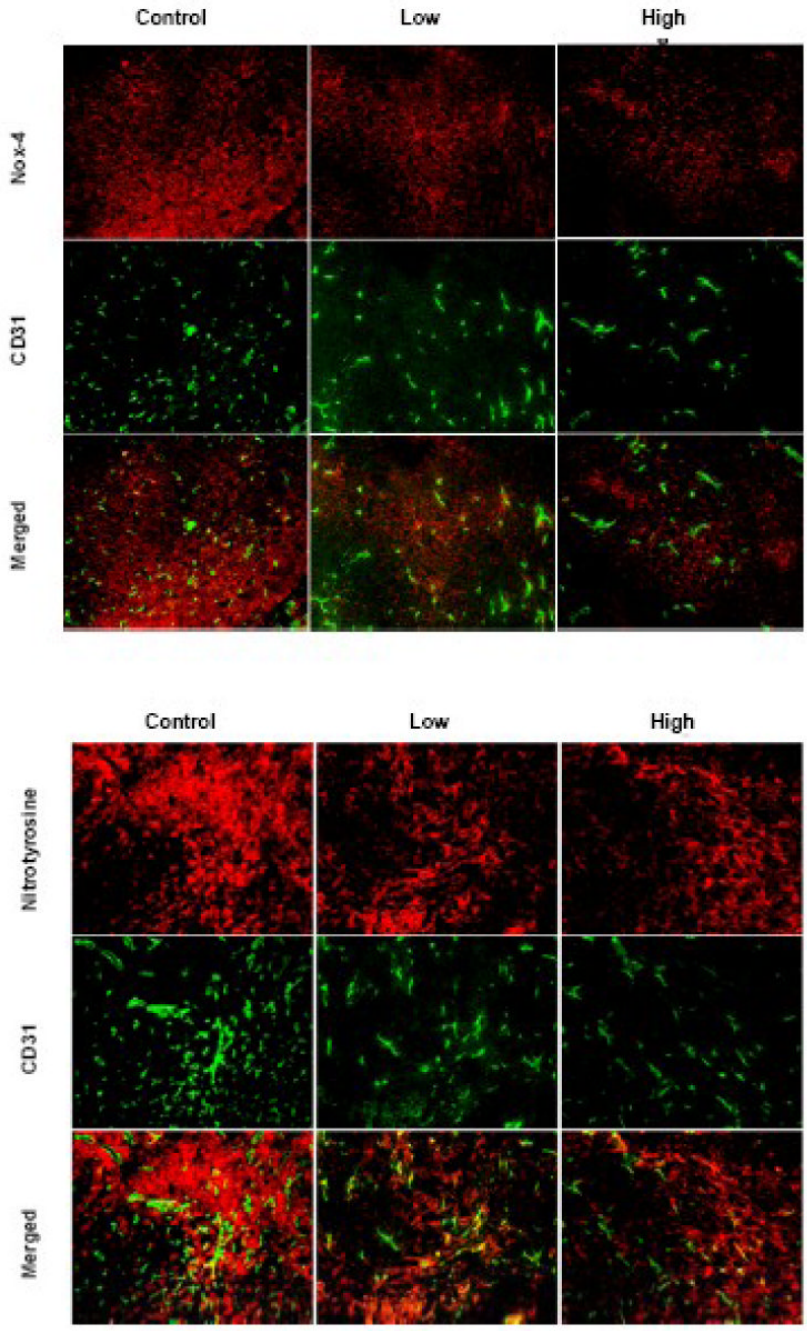

Figure 6. Co-localization of blood vessels with Nox-4 and 3-nitrotyrosine

Representative images of 4T1 stained either for CD31 pairing with Nox-4 and nitrotyrosine. Co-localization of Nox-4 and nitrotyrosine with CD31 displayed higher expression in angiogenic areas.

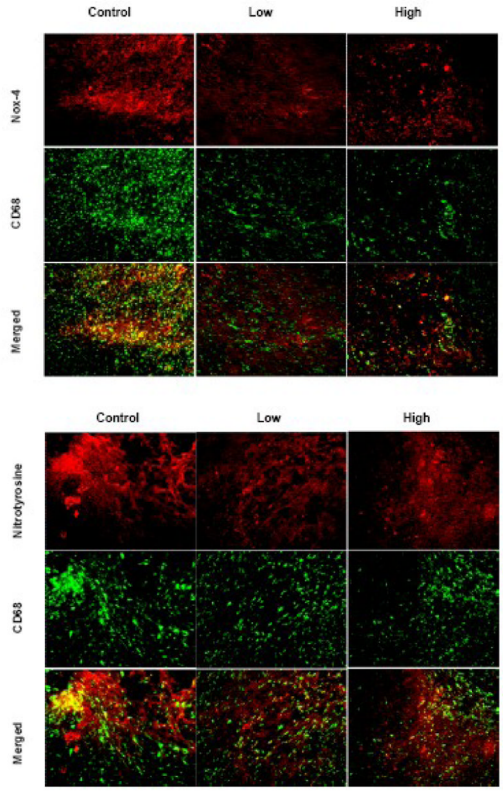

Figure 7. Co-localization of macrophages with Nox-4 and 3-nitrotyrosine

Representative images of 4T1 tumors stained for CD68 pairing with Nox-4 and nitrotyrosine. Co-localization of Nox-4 and nitrotyrosine with CD68 displayed higher expression in inflammatory spots.

Figure 8A

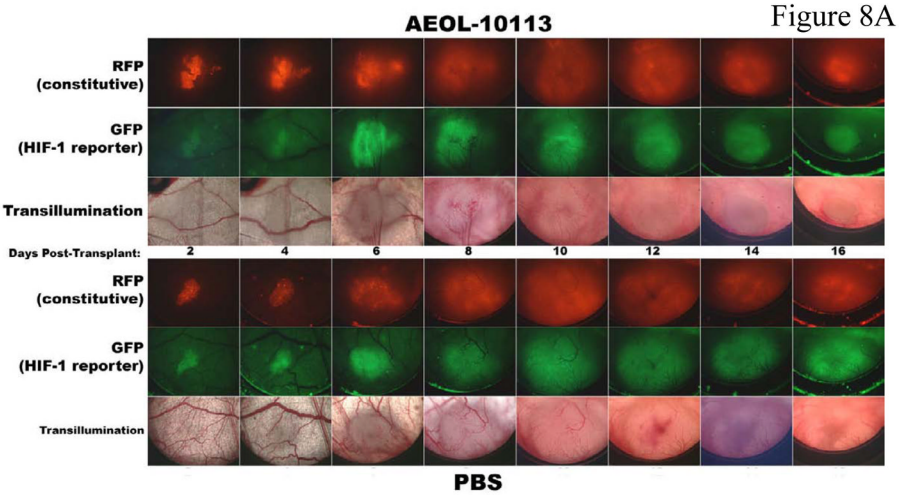

Figure 8B

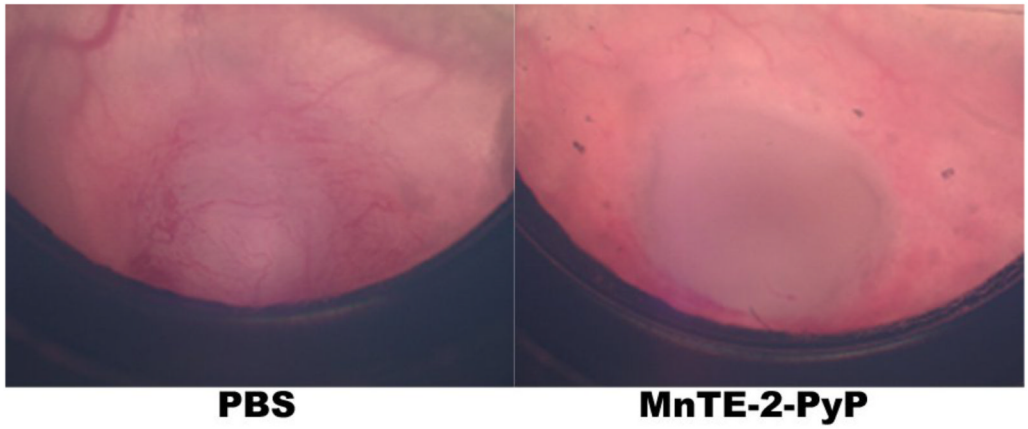

Figure 8C

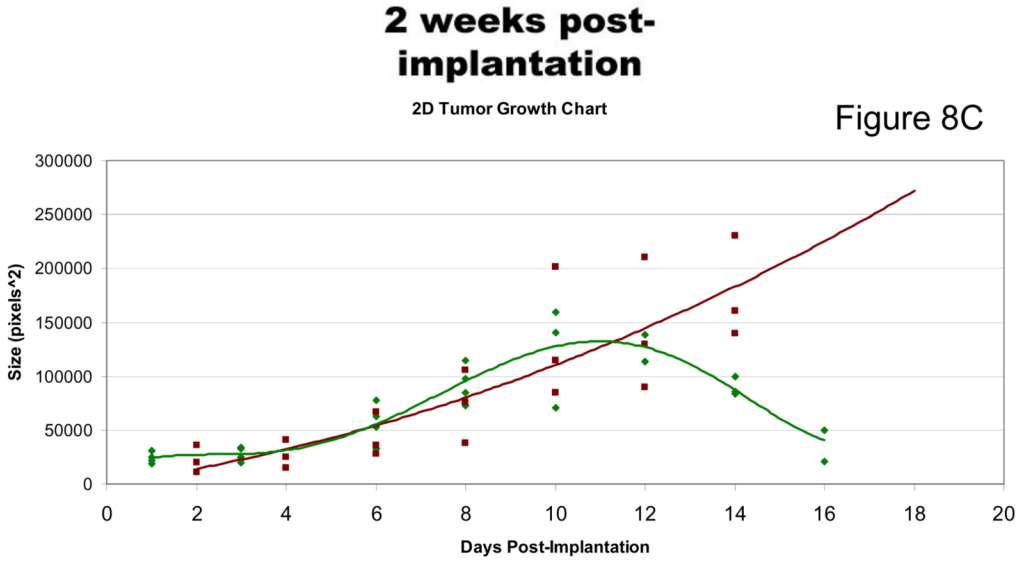

Figure 8. Intravital fluorescent monitoring of HIF-1 activity and tumor angiogenesis and tumor growth in a 4T1 window chamber study on BALB/c mouse with MnTE-2-PyP^{5+} (AEOL10113)

Drug was given at 6 mg/kg/day ip with 5 mice per group. A CMV-RFP construct was introduced into tumor that allowed expression of red fluoresecence protein (RFP) of a cytomegalovirus (CMV) promoter so that tumor cells can be tracked. Details are given in ref 18. The 4T1 line expresses also hypoxia responsive green fluorescent protein serving as a reporter for HIF-1α, which in turn allows a serial monitoring of HIF-1 activity levels by intravital fluorescence activity (Figure 8A and B). The growth curves (Figure 8C): green diamonds, MnTE-2-PyP^{5+}-treatment (AEOL10113), and the red square, PBS treatment.

Table 1

Levels of MnTE-2-PyP^{5+} in tumors after subcutaneous administration to Balb/C mice for 13 days at 2mg/kg/day and 15 mg/kg/day (given subcutaneously in two daily increments).

MnTE-2-PyP^{5+}	**tumor (*μg/g wet tissue)***
2 mg/kg/day	536 (SEM ± 43.58)
15 mg/kg/day	3139 (SEM ± 235.4)